Carpathian Journal of Earth and Environmental Sciences, August 2013, Vol. 8, No. 3, p. 27 - 42

CHEMOSTRATIGRAPHY, PETROGRAPHY AND REMOTE SENSING CHARACTERIZATION OF THE MIDDLE MIOCENE - HOLOCENE SEDIMENTS OF RAS BANAS PENINSULA, RED SEA COAST, EGYPT

Kamal ABOU ELMAGD[1], Ashraf EMAM[1] & Mohamed Wahbi ALI-BIK[2]

[1]*Aswan University, Geology Department, Faculty of Science, Aswan 81528, Egypt, Kamalali2@hotmail.com, ashrafemam99@hotmail.com*

[2]*National Research Centre, Geological Sciences Department, Cairo 12622, Egypt mwalibik2007@yahoo.com*

Abstract: Chemostratigraphic and petrographic investigations integrated with remote sensing lithologic mapping are used in harmony to discriminate and delineate the outcropping sedimentary successions at Ras Banas Peninsula, Red Sea coast. Tectonically, Ras Banas peninsula is considered as a part of Pre-Miocene continental slope. Their sedimentary successions account the sedimentation history from Middle Miocene up to Holocene which in part documents the deformational impacts that accompanied the Red Sea rifting. The Ras Banas sedimentary succession exhibits frequent unconformities and conspicuous lithologic variations comprising mixed siliciclastics/carbonate facies, evaporites, open marine and organic build up limestone as well as coral reefs, continental sandy gravels and beach sands. The carbonate succession at the area documents the highstand status of the Red Sea water from Middle Miocene to Pleistocene in accord to the global sea-level fluctuations. The chemical data of the studied rock units substantiates the field and petrographical results. On silica- lime- magnesia diagram, the syn-rifting mixed siliciclastics/carbonates are scattered between the quartz and dolomite reference points. The post-rifting carbonates are mainly pure dolostone, limestone and sandy limestone. Norm calculations indicate that the evaporites are mainly gypsum and anhydrite with substantial normative dolomite. The tectono-sedimentary evolution of Ras Banas sedimentary sequence in relation to Red Sea rifting phases and sea level fluctuations is discussed. New mapping was undertaken for the Ras Banas Peninsula using remote sensing and GIS techniques including band ratioing, principle component analysis and false color composition. Based on mineralogical data, special interest has been paid to the diagnostic spectral features that discriminate between evaporites and carbonates on one hand and between dolomite and calcite on the other.

Keywords: Ras Banas Peninsula, Chemostratigraphy, Remote Sensing, Carbonates, Evaporites.

1. INTRODUCTION

Along the full length of the Egyptian Red Sea coast a narrow maritime sedimentary sequence is juxtaposed to the Pan-African crystalline basement belt. The coastal plain section is composed mainly of Middle Miocene and subsequent younger sediments up to Recent (e.g. Beadnell, 1924; Said, 1962, 1990; Akkad & Dardir, 1966; Samuel & Saleeb-Roufaiel, 1977; Samuel & Cherif, 1978; Khedr, 1984; Philobbos et al., 1988; Felesteen et al., 1994; Mahran, 2000; Abou Elmagd & Emam, 2012). These sediments were accumulated in an elongated basin along rifted continental margin (Said, 1990). Everywhere along the Red Sea coastal plain, two sedimentary successions could reasonably be distinguished on the basis of the consequences of the Red Sea rifting processes. These are the syn-rifting deformed successions and post-rifting deformation-free rock units. The pre-rifting older sedimentary successions (Cretaceous – Eocene) outcrop only as structurally controlled outliers in the Quesir–Safaga district (Said, 1990).

The sedimentary Miocene and post-Miocene successions of the Red Sea coast uncomfortably overlay the Precambrian Pan-African crystalline basement rocks. In general, the Miocene sediments of the Red Sea coast were accumulated mainly in tectonically formed basins; consequently they exhibit frequent unconformities and great facies variation (Said, 1990); among them the Middle Miocene evaporaites (Abu Dabbab Fm) are conspicuous. The sedimentation of the studied Ras

Banas succession commenced in Middle Miocene and continued till Holocene. Hence, two main subdivisions could reasonably be distinguished in relation to the Red Sea rifting event: a) syn-rifting, deformed Middle Miocene successions and b) post-rifting, deformation-free (upper part of Middle Miocene to Recent) successions.

Turning to remote sensing applications, data acquired from remote sensors integrated with GIS techniques are of prime importance in many fields of geology such as mapping, mineral exploration and environmental studies. The geological applications of remote sensing data are based on the fact that each terrestrial component on the earth's surface has unique electromagnetic spectral characteristics. Consequently, the different rock units on the earth's crust are conventionally expected to display diagnostic electromagnetic spectra depending on their mineralogical compositions. During the past few decades, remote sensing data have been analyzed using several digital image processing techniques (image enhancement, fusion, band rationing, and principal component transformation) to carry out lithologic mapping and to identify mineral deposits in arid and semi-arid environments (e.g. Sultan et al., 1986; Chavez, 1989; Abrams & Hook, 1995; Sabins, 1997; Kusky & Ramadan, 2002; Gupta, 2003; Ranjbar et al., 2004; Al Rawashdeh et al., 2006; Gad & Kusky, 2007; Madani & Emam 2011; Ali-Bik et al., 2012).

The present study aims at investigating the chemostratigraphy, petrography and characteristics of sedimentary facies as well as applying remote sensing ETM+ data analysis to discriminate and delineate the different litho-facies in Ras Banas Peninsula. The geochemistry of Ras Banas sediments integrated with petrographic and stratigraphic investigations have been used to provide critical information regarding provenance, tectonic setting, and changes in depositional environment. New mapping (Fig. 1) is presented for the area, supported by remote sensing and GIS techniques, including PCA, band combinations and band rationing techniques.

2. MATERIALS AND METHODS

2.1. Field work, sampling, petrography and XRF

Many stratigraphic sections covering the whole sedimentary successions have been studied and sampled. Based on these data a complete stratigraphic column of Ras Banas sedimentary rocks is constructed (Fig. 2). Some representative samples covering the whole lithologic units were thin-sectioned and studied microscopically. Up to 66 representative samples of siliciclastics, carbonates (dolostone and limestone) and evaporites have been selected for whole-rock chemical analyses using XRF techniques. The powdered rock samples were prepared as fused beads and analyzed for major oxides against the suitable standard references for each rock type. The analyses were carried out at National Research Centre, Cairo, Egypt using an XRF Wavelength Dispersive Spectrometer (Axios Advanced, PANalytical 2005). Data were processed through advanced data treatment Software (IQ+ and Super Q).

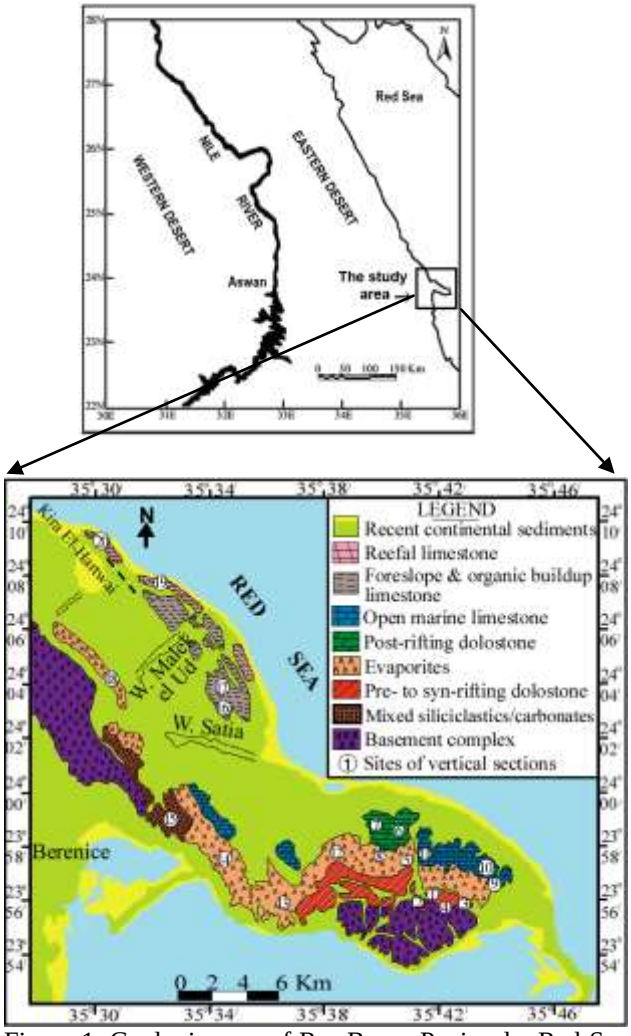

Figure 1. Geologic map of Ras Banas Peninsula, Red Sea Coast, as yielded from remote sensing and GIS techniques.

2.2. Remote sensing

For mapping and rock-unit discrimination purposes, three data sources were used in the present work including satellite images, digital topographic & geologic maps, and ground information. Digital image processing was applied to the Landsat Enhanced Thematic Mapper (ETM+) satellite image (Path/Raw 174/42), acquired in the year 2005. The

visible-near infrared (VNIR) and shortwave infrared (SWIR) bands acquired from Enhanced Thematic Mapper (ETM+) have been analyzed to discriminate between the different lithologic units that cropping out in Ras Banas Peninsula. The principal component analysis (PCA), RGB band combination and band rationing are the main remote sensing techniques applied during the present study. Data processing was managed via both ENVI (ver. 4.5) and Arc GIS (ver. 10) software. Digitized topographic and geologic maps were used for geometric correction of the satellite images and for some ground truth information.

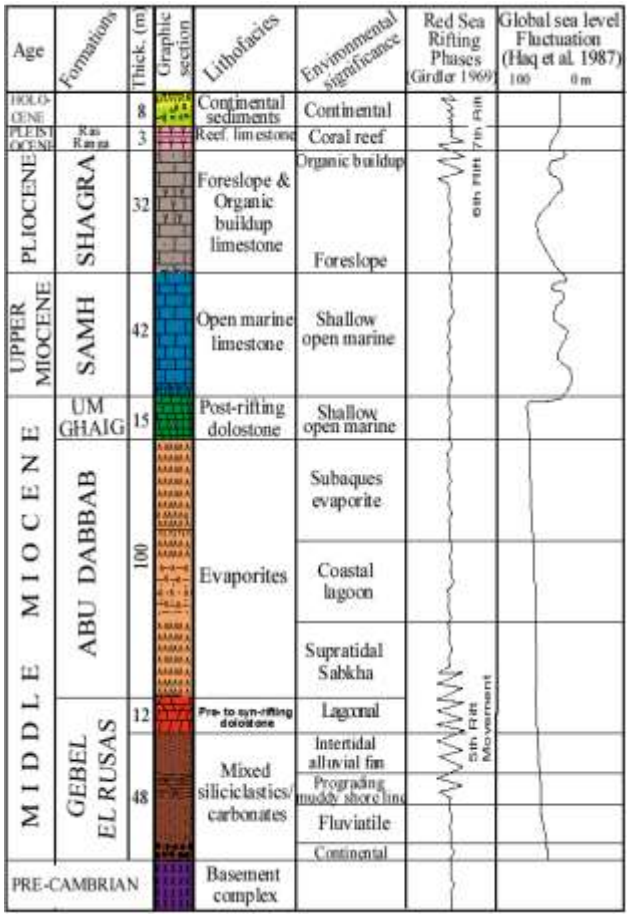

Figure 2. The compiled stratigraphic column, sedimentary environments and sea-level changes of Ras Banas Peninsula, modified after Felesteen et al., (1994).

3. RESULTS

3.1. Geologic setting

Ras Banas Peninsula is located on the Red Sea coast, between latitudes 23º 54′ N & 24º 10′ N and longitudes 35º 25′ E & 35º 46′ E (Fig. 1). The sedimentary sequence of Ras Banas Peninsula documents a time span from Middle Miocene to Holocene (Fig. 2). Structurally, they represent a simple NE trending monocline. Based on deformational history that is principally pertaining to the Red Sea rifting event, the sedimentary succession of the study area could be distinguished into two main subdivisions (Fig. 2): a) syn-rifting sequence (the lower units of the Middle Miocene section) that comprises both of Gebel El Rusas (mixed siliciclastic/carbonates) and Abu Dabbab (evaporites) formations, and b) post-rifting succession which include the topmost unit of the Middle Miocene section (Um Gheig Fm) in addition to Upper Miocene (Samh Fm) and subsequent Pliocene, Pleistocene and Holocene sediments.

The syn-rifting sequence overlies non-conformably the Precambrian crystalline basement and characterizes by frequent strike-slip and normal steep-dipping to near vertical faults. On the contrary, the post-rifting succession is generally horizontal without any deformational signs, except at the north-western part of the Peninsula, where an anticline is recorded and attributed probably to the plasticity of the underlying evaporites.

3.2. Sedimentary facies and petrography

The sedimentary sequence of Ras Banas Peninsula can be differentiated from bottom to top (Figs. 1 and 2) into the following rock types: (1) Syn-rifting mixed siliciclastic/carbonate rocks (Gebel El Rusas Fm) and evaporite rocks (Abu Dabbab Fm), (2) Post-rifting dolostone (Um Gheig Fm), (3) Shallow open marine limestone (Samh Fm) and (4) Sandy and reefal limestone (Shagra Fm) as well as silicified coral reef (Ras Ranga Fm) and beach gravel and sands.

3.2.1. Mixed siliciclastic/carbonate rocks (Gebel Rusas Fm)

In this rock-unit, the clastic sedimentary rocks are mainly sandstones and siltstones (attaining together about 45 m) that overlay unconformabably a polymictic conglomerate bed (~ 3 m). The sandstones and siltstones are frequently intercalated with carbonates and evaporites. A conspicuous gypsiferous claystone bed (~ 12 m) separates between fluviatile (~ 17 m) and intertidal alluvial fan (~ 16 m) environments. It represents prograding muddy shore line environment (cf. Fig. 2). Under the microscope, the sandstones are distinguished into greywacke and lithic wacke (Fig. 3 A). Their essential mineral constituents are quartz, lithic fragments, feldspars and micas (biotite & muscovite). Accessories are chlorite, kaolinite, manganese - and iron-oxides as well as epidote, rutile, garnet, zircon and tourmaline.

The carbonate component (~ 12 m thick) represents the upper part of Gebel El Rusas Formation, suggesting restricted to open shelf lagoonal environment (cf. Fig. 2). It is mainly dolostone (Fig. 3 B) whereas dolomite is mainly a secondary mineral formed at expense of pre-existing calcite. However, in carbonate/evaporite precipitation environment, endoevaporitic authigenic dolomite is expected to crystallize at suitable pH by the action of microbial bloom (e.g. Sanz-Montero et al., 2005; Ali-Bik et al., 2011). Dolomite crystals are often unzoned with cloudy centres and relatively clear rims. Pore-filling dolomite crystals are large (≥ 150 um long).

3.2.2. Evaporites

Evaporites of Abu Dabbab Formation (~ 100 m thick) are resting unconformably on the syn-rift dolostone of Gebel El Rusas Fm. (Fig. 2). Three gypsum facies encompassing subaerial (supratidal sabkha) and subaqueous varieties are recognized. Gypsum and anhydrite are the essential minerals in the studied evaporite sediments. Gypsum is also commonly present as pore-filling cement within clastics and dolostone of Gebel El Rusas Fm. Microscopically, gypsum crystals exhibit bird-tail, lenticular, prismatic, granular and daises shapes (Fig. 3 C & D). In field, two gypsum varieties are recorded including coarse selenite and very fine alabaster. Selenite occurs as tabular, colorless transparent crystals, which may reach 40 cm long. Alabaster occurs as lenses and irregular bodies at the uppermost part of some gypsum hills. This fine gypsum is very hard, massive, compact and tinted with grey color.

3.2.3. Post-rifting dolostone

This rock unit (~ 15 m thick) is represented by Um Gheig Formation (cf. Fig. 2). Microscopically, dolomite (Fig. 4 A) is the predominant phase and occurs as a secondary mineral at expense of pre-existing calcite. It occurs as unzoned crystals with cloudy centres and relatively clear rims.

3.2.4. Shallow open marine limestone (Samh Fm)

The sediments of Samh Formation (~ 42 m) are composed mainly of pure limestone varieties comprising algal and foraminiferal biosparite with rare silisiclastics (Fig. 4 B). Both field and microfacies investigations of these sediments refer to deposition in a shallow open marine environment.

3.2.5. Foreslope organic build up (Shagra Fm) and reefal limestones (Ras Ranga Fm)

These sediments are composed mainly of limestone varieties (attaining together about 35 m thick) with minor amount of sand-sized siliciclastics. The siliciclastic fractions within limestone beds are randomly distributed. Microscopically, the lower part of these sediments (Shagra Fm.) includes sandy algal biomicrite and biosparite (Fig. 4 C), referring to foreslope shallowing upward marine environment. The Ras Ranga Fm is composed of coralline algal, stomatolitic and reefal boundstones (Fig. 4 D), indicating deposition as an organic built up reef of platform margin (Wilson 1975).

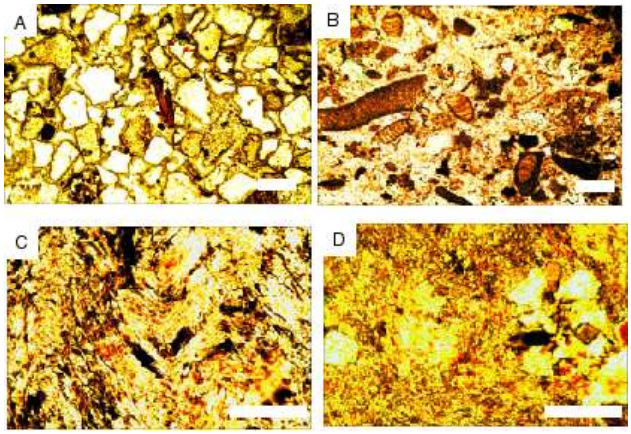

Figure 3. Photomicrographs of syn-rift sediments (scale bar 0.5 mm): (A) lithic wake, Gebel El Rusas Fm. (PPL). (B) Doloalgalsparite, upper part of Gebel El Rusas Fm. (PPL). (C) Primary gypsum shows bird-tail texture, Abu Dabbab Fm. (CN). (D) Lenticular gypsum confined daises of secondary porphyro-blastic gypsum, Abu Dabbab Fm. (CN).

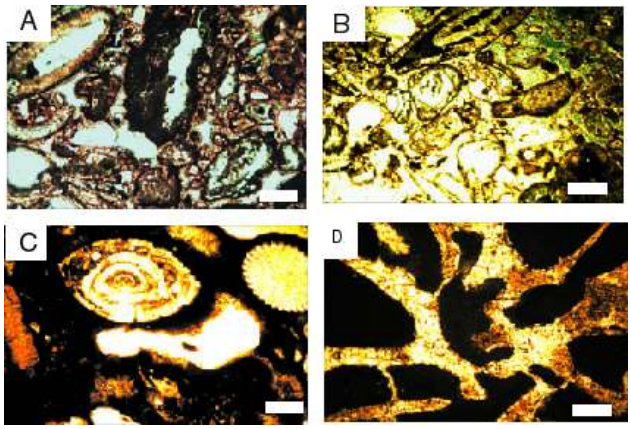

Figure 4. Photomicrographs of post-rift sediments (scale bar 0.5 mm): (A) Dolobiosparite, blue parts are dissolved voids, Um Gheig Fm (PPL). (B) Algal foraminiferal sparite, Samh Fm (PPL). (C) Limestone, biomicrite Shagra Fm (CN). (D) Limestone, reefal boundstone and secondary voids, Ras Ranga Fm (CN).

3.3. Chemostratigrphy

3.3.1. Chemical composition and characteristics

About 66 whole-rock samples covering a time span from Middle Miocene to Pleistocene have been

chemically analyzed (Table 1-3). Table 1 documents the chemical data of the syn-rifting mixed siliciclastics/dolostone (Gebel El Rusas Fm) and the evaporites (Abu Dabbab Fm). The normative components of the evaporites of Abu Dabbab Fm are given in table 2. Meanwhile, the chemical compositions of the post-rifting carbonate rocks (upper Middle Miocene to Pleistocene) are given in table 3.

Despite their stratigraphic position, the studied sediments exhibit a wide compositional variation. They encompass three main end-members: siliciclastics, carbonates (dolostone and limestone) and evaporites. The siliciclastics form the lower part of the Gebel El Rusas Formation (Fig. 2), where they overlie non-conformably the Precambrian crystalline basement rocks. They are characteristically intercalated with carbonates as noted in Table 1. Only samples with SiO_2 content > 61 % will be employed to deduce their probable chemical nomenclature. On plotting on the classification diagram of Wimmenaure (1984), the studied samples exhibit a rather limited range of K_2O/Na_2O and are scattered into the fields of Qz-rich greywacke and greywacke (Fig. 5). On the classification diagram of Wintsch and Kvale (1994), they consistently plot into the fields of lithic arenite, greywacke and subarkose (Fig. 6). On the provenance discrimination diagram of Roser & Korsch (1988) – not shown here- they suggest a polycyclic siliciclastic provenance.

Similarly, the dolostone which constitutes the upper part of Gebel El Rusas Fm is conspicuously enriched in SiO_2 content (up to 20%) and exhibits rather wide ranges of MgO (14.46-23.83 wt.%), CaO (27.51-46.20 wt.%) and Na_2O (0.42-2.69 wt.%). Regarding the evaporite rocks of Abu Dabbab Fm, they are obviously intercalated mainly by carbonates and to lesser extent by silt (Tables 1 and 2). They are mainly gypsum and anhydrite. The calculated normative gypsum component in gypsum samples varies from 81 to 70 %, while the normative anhydrite component in anhydrite samples ranges from 76 to 67 %. The intercalated calcite component in gypsum samples ranges from 5 to 16 %, while the normative dolomite content attains ~ 12%. Similarly, the anhydrite samples contain up to 20% calcite and 25% dolomite. Beside gypsum and anhydrite, there are subordinate contents of silt, dolomite and calcite forming dolomitic limestone, calcareous dolostone and dolomitic silty limestone (Table 1). In terms of facies variability, the samples of coastal sabkhas (section 5 in Tables 1 and 2) are characterized by higher aggregate content as expected in such environment. Gypsum and anhydrite contents in samples of both lagoonal and subaqueous facies are relatively higher (cf. Tables 1 and 2). Generally speaking, the observed clastic input and the mutual distribution of both dolomite and calcite on one hand and gypsum and anhydrite on the other hand might indicate sedimentation, evaporitic precipitation and diagenesis in environment characterized by tectonic disturbance and sea level fluctuation.

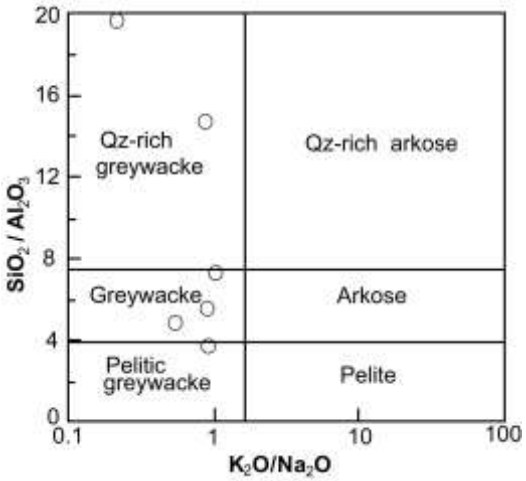

Figure 5. Composition of the sandstones of Gebel El Rusas Fm in the classification diagram after Wimmenauer (1984).

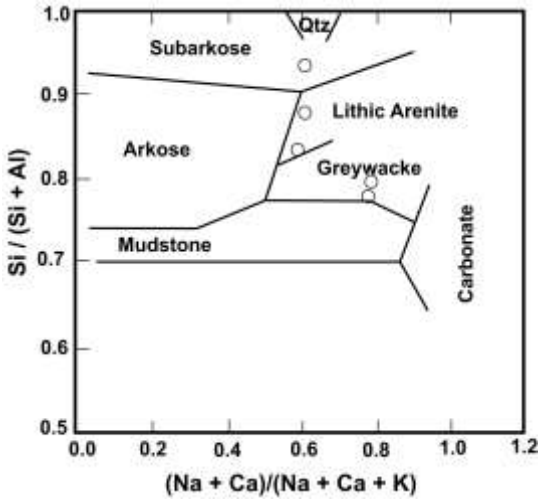

Figure 6. Composition of the sandstones of Gebel El Rusas Fm in the classification diagram of sedimentary rocks after Wintsch & Kvale (1994).

The post-rifting dolostone (Um Gheig Fm) is almost pure, compared to that of the syn-rifting varieties of Gebel El Rusas Fm, whereas it exhibits rather narrow ranges of MgO, CaO and Na_2O (cf. Tables 1 and 3). The limestone of the Samh Fm (Upper Miocene) is conspicuously pure with CaO content of 47.7 to 55.5 wt. %, in comparison with that of Shagra Fm (Pliocene) as given in Table 3; the latter contains up to 17.39 wt % SiO_2 and CaO content of 18.6 to 53.7 wt.%. The limestone of Ras

Ranga Fm (Pleistocene) varies from pure limestone to silty limestone.

3.4. Remote sensing

In general, the essential minerals of studied sedimentary rocks are calcite, dolomite, gypsum and anhydrite. Each of these minerals has its own diagnostic absorption feature; hence its characteristic spectra (e.g. Hunt & Salisbury, 1970; 1971; Hunt, 1982; Crowley, 1986; Howari, 2002). Tracing the diagnostic absorption features of these minerals and using different application techniques of remote sensing data such as band rationing and principle component analysis, the rock-units of Ras Banas peninsula are successfully discriminated and new mapping is presented for the area (Fig. 1). The basis and details of the discrimination process are given in the discussion section.

4. DISCUSSION

4.1. Tectono-sedimentary evolution and chemo-stratigraphy of Ras Banas sediments

Tectonically, Ras Banas peninsula is considered as a part of Pre-Miocene continental slope (Abdel Gawad, 1969; Schandelmeier et al., 1987; Meshref, 1990). In general, the Miocene sediments of the Red Sea coast were deposited mainly in tectonically formed basins; consequently exhibit frequent unconformities and great facies variations (Said, 1990). At Ras Banas Peninsula, there are six unconformity surfaces; the oldest one separates the Precambrian basement rocks from the overlying Middle Miocene sediments. The other unconformity surfaces separate between the different stratigraphic units (cf. Fig. 2), supporting cyclic sedimentation in tectonically unstable – at least during lower Middle Miocene- environment. Ras Banas sedimentary successions account the sedimentation history from Middle Miocene up to Holocene. They documents in part the rifting event of the Red Sea and could be reasonably distinguished into two main subdivisions (cf. Fig. 2):

4.1.1. Syn-rifting units

The syn-rifting, deformed sequences are represented by the mixed siliciclastics/carbonates (Gebel El Rusas Fm) and the evaporites of Abu Dabbab Fm. The recorded deformational patterns in the Middle Miocene section of Ras Bans area follow – in general - the main ancient faulting trends in the older rocks of the south-eastern part of Egypt. These ancient fractures and shears most probably originated in response to many successive compressive and/or extension forces, since the Precambrian and culminated in the Red Sea rifting.

The mixed siliciclastics/carbonate rock-unit of Gebel El Rusas Fm exhibits variable depositional systems (continental, marine and transitional) and tectonically unstable sub-environments (cf. Fig. 2) that were greatly impacted by both local tectonic unrest and global sea level-fluctuation. The continental clastic components of this rock-unit imply cycles of sedimentation in different depositional environments. They encompass basal polymictic conglomerates and cycles of fluviatile and intertidal alluvial fan sandstones with intercalation of gypsiferous claystones during prograding muddy shoreline. The basal conglomerates indicate accumulation in high-energy environment. The gravel and other clasts were derived most probably from the nearby crystalline basements, while sandstones seem to be recycled products of pre-existing siliciclastic sources.

The carbonates were deposited in lagoonal depositional system implying calm environment along the shoreline of a siliciclastic continental shelf. Generally speaking, the extension of the carbonates at the area documents the highstand status of the Red Sea water from Middle Miocene to Pleistocene in accord to the global sea-level fluctuation. The carbonate rocks of Gebel El Rusas Formation are almost totally dolostone with substantial amount of quartz. The dolostone is most probably evolved at expense of the pre-existing limestone. Dolomitization of the latter could probably be linked with the succeeding evaporites (Abu Dabbab Fm), i.e. by the action of the subaerial brine reflux (e.g. Boggs, 2001).

Turning to chemical data, the samples of Gebel El Rusas Formation (mixed siliciclastics/ carbonates) are scattered between the quartz and dolomite reference points (Fig. 7), exhibiting heterogeneous composition and supporting the field and microscopic investigations.

The siliciclastic/carbonate rock-unit is succeeded upwards by the Middle Miocene evaporites (Abu Dabbab Fm). These evaporites comprise subaerial and subaqueous gypsum and anhydrite deposits, which developed in supratidal sabkha and shoal environments, respectively. Primary gypsum occurs in different forms (tabular and lenticular gypsum) and sizes (selenite and alabaster) implying evolution under varying salinities in environment characterized by microbial bloom. In general, the large selenite crystals evolve in higher salinity in contrast to fine gypsum, implying formation during hot seasons (e.g. Ali-Bik et al., 2011).

Table 1. Chemical analyses of the syn-rifting mixed siliciclastics/carbonates (Gebel El Rusas Formation) and evaporites (Abu Dabbab Formation), Ras Banas Peninsula.

Formation	Lithology	Section No. & Sample No.	SiO_2	TiO_2	Al_2O_3	Fe_2O_3	MnO	MgO	CaO	Na2O	K2O	P_2O_5	L.O.I.	Total	Facies
Gebel El Rusas Fm	Dolostone	*Sec. 1-1	5.65	0.06	0.36	0.39	0.01	20.77	34.54	0.52	0.17	0.08	37	99.55	Mixed Siliciclastic /carbonates (dolostone)
	Dolostone	Sec. 1-2	8.01	0.16	1.81	1.25	0.03	19.32	31.12	1.07	0.47	0.08	36.13	99.43	
	Dolostone	Sec. 1-3	12.64	0.13	0.34	0.14	0.07	21.83	46.2	2.56	0.29	0.04	15.68	99.93	
	Dolostone	Sec. 2-1	12.94	0.04	0.91	0.3	0.01	18.51	28.65	0.44	0.01	0.04	38.14	99.99	
	Dolostone	Sec. 2-2	8.43	0.17	1.9	1.32	0.03	18.23	30.2	1.13	0.49	0.08	38.03	99.51	
	Dolostone	Sec. 2-3	5.95	0.06	0.38	0.41	0.01	20.81	32.62	0.55	0.18	0.08	38.94	99.82	
	Dolostone	Sec. 3-1	13.31	0.14	0.36	0.15	0.08	22.98	43.48	2.69	0.3	0.04	16.51	99.74	
	Dolostone	Sec. 3-2	20.16	0.09	0.93	0.51	0.02	15.22	27.51	1.23	0.17	0.04	34.12	99.83	
	Dolostone	Sec. 4-1	19.16	0.09	0.89	0.49	0.02	14.46	30.44	1.17	0.16	0.04	32.41	99.31	
	Dolostone	Sec. 4-2	12.29	0.04	0.86	0.29	0.01	18.58	30.58	0.42	0.01	0.04	36.23	99.36	
	Dolostone	Sec. 4-3	12.64	0.13	0.34	0.14	0.07	23.83	43.37	2.56	0.29	0.04	15.68	99.1	
	Dolostone	Sec. 4-4	13.31	0.14	0.36	0.15	0.08	22.98	43.48	2.69	0.3	0.04	16.51	99.74	
	Silty dolostone	Sec. 14-1	35.73	0.46	1.82	0.89	0.47	16.55	33.84	1.82	0.4	0.08	7.02	99.08	
	Calcareous siltstone	Sec. 14-2	52.76	0.39	2.31	0.56	0.33	6.02	24.36	2.31	1.68	0.03	8.3	99.03	
	Dolomitic sandstone	Sec. 14-3	45.73	0.5	1.82	0.73	0.21	16.83	23.84	1.38	0.36	0.98	7.11	99.49	
	Dolomitic sandstone	Sec. 14-4	48.73	0.41	1.76	0.68	0.42	15.15	20.84	1.73	0.86	0.1	9.02	99.7	
	Siltstone	Sec. 15-1	73.4	0.25	13.4	1.82	0.08	1.46	1.84	3.04	2.97	0.14	1.37	99.77	
	Siltstone	Sec. 15-2	61.12	0.27	16.3	4.08	0.14	3.22	6.24	2.04	1.98	0.37	4.18	99.94	
	Sandy siltstone	Sec. 15-3	72.05	0.24	15.23	1.45	0.57	2.87	2.7	1.66	0.95	0.81	1.1	99.63	
	Sandstone	Sec. 15-4	71.03	0.82	9.84	5.84	0.07	1.75	1.79	1.94	2.11	0.1	3.95	99.24	
	Sandstone	Sec. 15-5	80.05	0.25	5.49	2.48	0.15	0.9	0.98	1.98	1.83	1.01	4.1	99.22	

Table 1. Continued (Abu Dabbab Fm). The given lithology is based on the calculated normative components in Table 2.

Formation	Lithology	Section No. & Sample No.	SO_3	H_2O at 250 °C	CaO	SiO_2	TiO_2	Al_2O_3	Fe_2O_3	MnO	MgO	Na_2O	K_2O	P_2O_5	L.O.I.	Facies
	Dolomitic calcareous anhydrite	Sec. 5-1	38.56	--	43.15	1.16	0.09	--	0.50	0.07	2.57	2.00	0.38	0.04	13.45	
Abu Dabbab Fm	Gypsum	Sec. 5-2	40.50	9.12	34.58	4.16	0.06	1.63	0.06	0.23	1.83	0.5	0.15	0.09	7.50	Evaporites
	Anhydrite	Sec. 5-3	40.62	--	42.51	1.14	0.09	--	0.5	0.07	2.53	1.97	0.37	0.71	10.39	
	Dolomitic silty limestone	Sec. 5-4	--	--	33.75	30.74	0.07	7.05	--	0.93	4.60	0.73	0.07	0.08	21.94	
	Dolomitic silty limestone	Sec. 5-5	--	--	37.34	21.31	0.05	4.89	--	0.65	3.19	0.51	0.05	0.05	32.79	
	Calcareous gypsum	Sec. 8-1	35.86	8.07	37.51	1.10	0.05	--	--	0.09	2.58	1.95	0.17	0.04	12.54	
	Gypsum	Sec. 8-2	40.61	9.14	35.96	1.06	0.05	--	--	0.09	2.47	1.87	0.17	0.09	17.72	
	Gypsum	Sec. 8-3	41.50	9.23	35.39	0.63	0.07	1.64	--	0.16	1.74	0.23	0.08	0.05	9.14	
	Calcareous dolostone	Sec. 12-1	3.00	0.68	39.86	2.73	0.01	--	--	0.08	9.56	4.39	0.24	0.06	40.75	
	Dolomitic limestone	Sec. 13-1	--	--	52.71	--	0.04	--	--	0.49	3.59	1.24	0.06	0.08	42.38	
	Dolomitic anhydrite	Sec. 13-2	43.28	--	36.27	--	0.07	--	--	0.76	5.53	1.92	0.09	0.08	12.08	
	Gypsiferous lime	Sec. 18-1	20.50	--	43.51	3.24	0.06	0.39	0.42	0.07	2.78	2.24	0.33	0.01	26.18	

* Sec. 1-1: Vertical section number followed by bed number from the top of the section. Samples of section 5 refer to coastal sabkhas and those of section 8 represent the lagoonal evaporites. Subaqueous evaporites are represented by the samples of the sections 8, 13 and 18.

Table 3. Chemical composition of post-rifting carbonates (upper Middle Miocene to Pleistocene), Ras Banas Peninsula.

Formation	Lithology	Section No. & Sample No.	SiO_2	TiO_2	Al_2O_3	Fe_2O_3	MnO	MgO	CaO	Na_2O	K_2O	P_2O_5	L.O.I.	Total	Facies
Ras Ranga Fm.	Silty Limestone	Sec. 19-1	11.8	0.07	0	5.55	0.14	2.78	27.8	6.31	1.32	0.13	43.5	99.53	Limestone
	Limestone	Sec. 19-2	3.06	0.01	0.87	0.19	0.01	1.04	51.5	0.18	0.01	0.02	42.7	99.66	
	Limestone	Sec. 20-1	1.16	0.01	2.32	0.19	0.12	1.09	52.7	0.11	0.01	0.08	42.0	99.9	
	Limestone	Sec. 20-2	1.04	0.02	0.53	0.14	0.05	1.82	53.7	0.12	0.03	0.04	42.3	99.9	
	Limestone	Sec. 20-3	0.57	0	0.79	0.23	0.39	0.97	53.5	0.21	0.01	0.05	43.1	99.8	
Shagara Fm.	Sandy Limestone	Sec.16-1	17.3	0.03	1.18	0.27	0.01	5.75	38.5	0.23	0.08	0.04	36.3	99.9	
	Sandy Limestone	Sec.17-1	16.2	0.05	0.01	0.32	0.01	1.0	45.2	0.5	0.16	0.04	36.4	99.9	
	Sandy Limestone	Sec. 17-2	20	0.3	11.0	0.7	0.06	4.69	18.6	11.0	0.78	0.02	32.2	99.5	
Samh Fm.	Limestone	Sec. 9-1	0.27	0	0.15	0.07	0.01	1.01	54.2	0.21	0.06	0.02	43.6	99.6	
	Limestone	Sec. 9-2	2.09	0.01	1.9	0.21	0	0.94	52.7	0.52	0.2	0.01	41.0	99.6	
	Limestone	Sec. 9-3	1.57	0.05	0.7	0.22	0.01	1.63	52.3	0.4	0.01	0.03	42.9	99.8	
	Limestone	Sec. 9-4	1.67	0.02	0.31	0.22	0.01	8.33	47.7	0.57	0.1	0.03	40.4	99.5	
	Limestone	Sec. 10-1	3.6	0.06	1.83	0.34	0.01	0.71	51.8	0.54	0.09	0.02	40.5	99.5	
	Limestone	Sec. 10-2	3.29	0.05	1.14	0.33	0.01	0.64	50.0	1.99	0.06	0.01	42.1	99.6	
	Limestone	Sec. 10-3	0.42	0.02	0.74	0.06	0	4.4	51.5	0.54	0.05	0.06	41.8	99.7	
	Limestone	Sec. 10-4	0.27	0.01	1.43	0.04	0	3.97	51.2	0.43	0.2	0.06	42.0	99.7	
	Limestone	Sec. 10-5	0.3	0	1.06	0.02	0	2.21	52.6	0.46	0.1	0.02	42.7	99.6	
	Limestone	Sec. 11-1	0.51	0.01	2.22	0.12	0.15	0.55	53.1	0.21	0.05	0.08	42.4	99.4	
	Limestone	Sec. 11-2	0.17	0	0.51	0.02	0.1	0.41	55.5	0.31	0.15	0.03	42.2	99.4	
	Limestone	Sec. 11-3	0	0.04	0	0	0.49	3.09	51.7	1.24	0.06	1.45	41.8	99.9	
	Limestone	Sec. 11-4	0.3	0	1.33	0.03	0	1.4	53.7	0.41	0.23	0.03	42.4	99.8	
Um Gheig Fm.	Dolostone	Sec. 6-1	0.8	0	0	0.62	0.51	20.1	35.2	0.32	0.14	0.13	42.1	99.8	Dolostone
	Dolostone	Sec. 6-2	2.51	0.04	1.45	0.58	0.02	19.4	33.3	1.07	0.18	0.04	41.3	99.8	
	Dolostone	Sec. 6-3	1.49	0.02	0.35	0.22	0.04	20.6	36.7	0.27	0.08	0.1	40.0	99.9	
	Dolostone	Sec. 6-4	2.32	0.04	0.35	0.47	0.02	21.2	32.8	0.96	0.17	0.04	41.5	99.8	
	Dolostone	Sec. 6-5	1.56	0.02	0.97	0.27	0.01	16.5	38.2	0.88	0.08	0.04	41.3	99.9	
	Dolostone	Sec. 6-6	3.21	0.05	0.55	0.88	0.35	20.1	33.1	1.06	0.08	0.08	40.3	99.9	
	Dolostone	Sec. 7-1	0.75	0.02	0.26	0.12	0.13	16.1	40.0	0.53	0.09	0.03	41.9	99.9	
	Dolostone	Sec. 7-2	3.38	0.02	0.77	0.17	0.01	19.1	32.7	0.67	0.08	0.03	42.9	99.9	
	Dolostone	Sec. 7-3	3.34	0.05	0.78	0.65	0.01	18.6	33.4	1	0.32	0.03	41.7	99.6	
	Dolostone	Sec. 7-4	3.63	0.05	0.77	0.72	0.5	21.6	31.7	0.09	0.03	0.08	40.7	99.9	
	Dolostone	Sec. 7-5	1.29	0.02	0.35	0.42	0.04	21.9	35.4	0.27	0.08	0.1	40.0	99.9	
	Dolostone	Sec. 7-6	1.56	0.02	0.97	1.27	0.01	17.7	37.0	0.88	0.08	0.04	40.3	99.9	

The lenticular-gypsum form is attributed to interaction of biogenic crystallization inhibitors (e.g. Cody & Cody, 1989; Ali-Bik et al., 2011). Specific microbial blooms such as algae excrete certain organic molecules (enzyme α-analyze) that are capable to produce the lenticular gypsum-form by decreasing the growth of gypsum crystals in c [001] direction (Cody & Cody, 1989 and references therein).

Table 2. The calculated normative composition of evaporites (Abu Dabbab Fm) from the given data in Table1. The sum of R_2O_3, SiO_2, TiO_2 and P_2O_5 are reported as aggregates, representing the accessories such as siliciclastics and iron-oxides.

Section No. & Sample No.	Gypsum %	Anhydrite %	Dolomite %	Calcite %	Aggregates %	Total
5-1	--	67.0	10.5	20.5	2.0	100
5-2	80.1	--	8.7	4.8	6.4	100
5-3	--	76.2	11.1	10.60	2.1	100
5-4	--	--	21.0	40.2	38.8	100
5-5	--	--	14.6	58.6	26.9	100
8-1	70.6	--	12.1	16.1	1.2	100
8-2	79.8	--	11.5	7.4	1.2	100
8-3	81.3	--	8.2	7.8	2.7	100
12-1	6.0	--	45.6	45.5	2.9	100
13-1	--	--	16.1	83.4	0.5	100
13-2	--	73.8	25.4	--	0.8	100
18-1	--	35.4	13.1	47.2	4.3	100

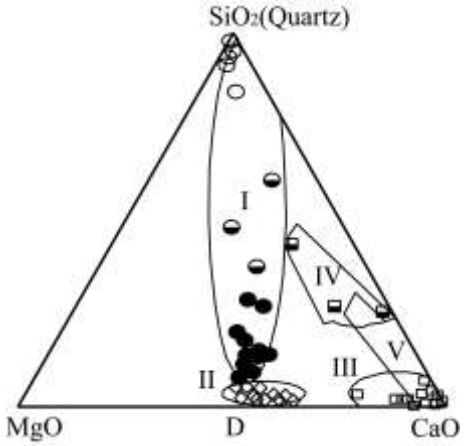

Figure 7. SiO_2 – MgO – CaO (All as mole %) triangle diagram for the studied Ras Banas sedimentary successions (Middle Miocene to Pleistocene). Symbol D denotes the dolomite reference point. Field I (Gebel El Rusas Fm), Field II (Um Gheig Fm), Field III (Samh Fm), Field IV (Shagra Fm) and Field V (Ras Ranga Fm).

4.1.2. Post-rifting units

The Um Gheig Fm represents the base of the post-rifting succession of the area (Fig. 2) and is composed of almost pure dolostone that implies shallow open marine environment. It is free of quartz in comparison to the syn-rifting siliceous dolostone of Gebel El Rusas Fm. Again, the dolostone was formed by the dolomitization of the pre-existing limestone either by the interaction of meteoric porewaters in a mixing-zone with the marine porewaters (mixing-zone model) or by the involvement of the marine porewaters in response to the sea-level rising (e.g. Boggs, 2001). Chemically, it is pure and clustered around the dolomite reference point (Fig. 7).

The Um Gheig Fm is followed upward by Samh Fm (Upper Miocene) which is composed of limestone, stromatolitic limestone and sandy limestone, implying shallow open marine environment (Fig. 2). Pliocene sediments are represented by Shagra Formation, which is formed of sandy limestone, coralline and stromatolitic limestones, suggesting foreslope and organic build up environment. The Pleistocene sediments are represented by silicified coral reefs (Ras Ranga Formation), while the Holocene sediments are represented by raised coral reefs, sandy ravels and beach sands. The chemical data as presented in Table (3) and Fig. (7), is in close agreement with field and microscopic data. The samples of Samh Fm (Upper Miocene) are almost pure limestone, while those of the Shagra Fm (Pliocene) are considerably shifted towards the quartz apex. It might be related to the observed disturbance on the Girdler's (1969) curve (Fig. 2), reflecting most probably local unrest in terms of intense quakes. The samples of Ras Ranga Fm (Pleistocene) are compositionally clustered mainly around CaO apex (Fig. 7); only few samples are contaminated by silica.

4.2. Remote sensing

4.2.1. Band Rationing

Band ratios and multiplications are remote sensing techniques that maximize the rock discrimination in landsat images (e.g. Sultan et al., 1986; Sabins 1997; Kusky & Ramadan, 2002; Inzana et al., 2003; Ali-Bik et al., 2012) where specific band ratios can clarify the relative small difference in spectral behaviour (reflectance and absorption) of different minerals at certain wavelength. The rock-forming minerals have unique responses in interaction with electromagnetic radiation. Each mineral has a diagnostic spectral signature or spectral response curve (e.g. Gupta, 2003). Absorption features of minerals in different

regions of the spectral response curve are caused by occurrence of anion groups such as SO_4, CO_3, hydroxyl ion (OH) and water molecule (H_2O). Accordingly, carbonate and evaporite minerals have diagnostic spectral signatures or spectral features, as a result of their interaction with electromagnetic radiation, distinguishing them from the other minerals (Huang & Kerr, 1960; Hunt & Salisbury, 1971; Gaffey, 1985; 1986; 1987; Crowley, 1986; Van der Meer, 1994; 1995; Gupta, 2003).

The whole Ras Banas sedimentary section is composed of three main lithologic types: siliciclastics, carbonates and evaporites. Carbonate minerals have diagnostic absorption features at 2.30-2.35µm and 2.50-2.55µm due to CO_3^{-2} ion. So, these absorption features have been used to discriminate carbonate minerals from other minerals and identify calcite- and dolomite-bearing rocks on the earth surface (Fig.8). Hunt & Salisbury (1971) found that calcite shows absorption feature at 2.35µm and dolomite has absorption feature at 2.33µm, i.e. within the wavelength range of ETM band7 (2.08–2.35µm). Also, evaporite minerals can be distinguished by examining absorption features through their spectral response curves (Hunt & Salisbury, 1970; Hunt, 1982; Crowley, 1991). The water molecules in the structure of gypsum affect the infrared spectrum between 1.0 and 2.5µm, where the spectral response curve of gypsum (Fig. 8) shows diagnostic absorption features at 1.4µm, 1.55µm, 1.75µm, 1.9µm and 2.3µm (Howari, 2002). This means that sulfate-evaporites, especially gypsum, show sharp absorption features in ETM infrared band5 (1.55–1.75µm) and band7 (2.08–2.35µm). Thus, band rationing technique using band 5 and band 7 is useful to discriminate between carbonates and sulfate-evaporites of Ras Banas. The processed band ratio (5/7) image clearly differentiates the carbonate rocks and sulfate-evaporites (Fig. 9). The carbonates show bright tone due to their high reflectance features in band 5 and high absorption features in band 7. On contrast, the sulfate-evaporites have absorption features in both band 5 and band 7, so that they show medium to dark gray tone.

4.2.2. Crosta PC Analysis

The principal component analysis (PCA) is a multivariate statistical technique that selects uncorrelated linear combinations (eigenvector loadings) of variables in such a way that each successively extracted linear combination, or principal component (PC), has a smaller variance (Singh & Harrison, 1985). The main objective of PCA is to remove redundancy in multispectral data. It is widely used in geology as an image processing approach. Important advantages of the PCA are the facts that the new principal component images are often more interpretable than the original data (Jensen, 1986), and that the informational content can be compressed in a fewer number of bands. The PCA allows identification of the principal components that contain spectral information about specific minerals, as well as the contributions of the original bands to the components in relation to the spectral response of the minerals under consideration. In this context, Crosta technique (e.g. Crosta & Moore, 1989; Loughlin, 1990; 1991), which is also known as Feature-Oriented Principal Component Selection (FPCS), is widely used. It discriminates different materials either as bright or dark pixels in the principal components according to the magnitude and sign of the eigenvector loadings.

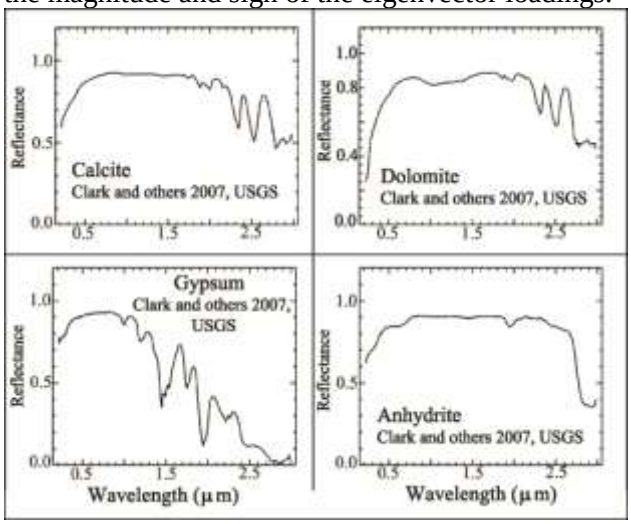

Figure 8. Spectral features of calcite, dolomite, gypsum and anhydrite in the visible-near infrared (VNIR) and shortwave infrared (SWIR) regions.

The Crosta technique is applied in the present work on four ETM bands (visible bands 2, 3, and shortwave infrared bands 5, 7), taking into account only the bands that exhibit spectral features (reflectance/absorption) caused by CO_3-, SO_4- and H_2O-bearing minerals. The resultant four PCs of Crosta technique are illustrated in (Table 4), where the first component encompasses the brightness information, sometimes called albedo. It is clear that PC1 has positively high eigenvector loadings for all four ETM bands, and contains about 96.7% of the total data variation. So, its gray-scale PC-image failed to discriminate between different litho-facieses, but it exhibits information about the elevation and geomorphology of the area. The second and all other subsequent principal components encompass divergences in spectral reflectance among surface materials which depend on their mineralogical and chemical characteristics.

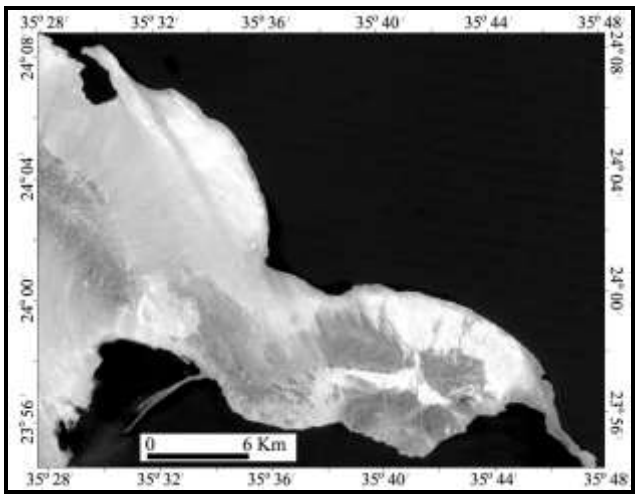

Figure 9. Gray-scale band ratio (5/7) image showing the carbonate rocks with bright tone.

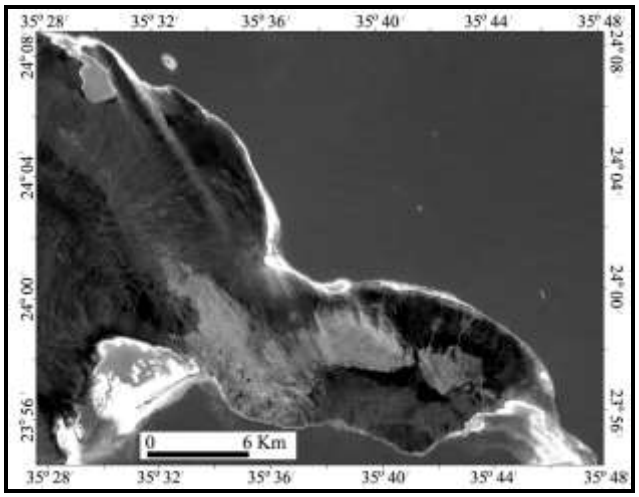

Figure 10. Gray-scale PC2-image discriminates clearly between carbonates (dark tone) and sulfate-evaporites (light-gray tone).

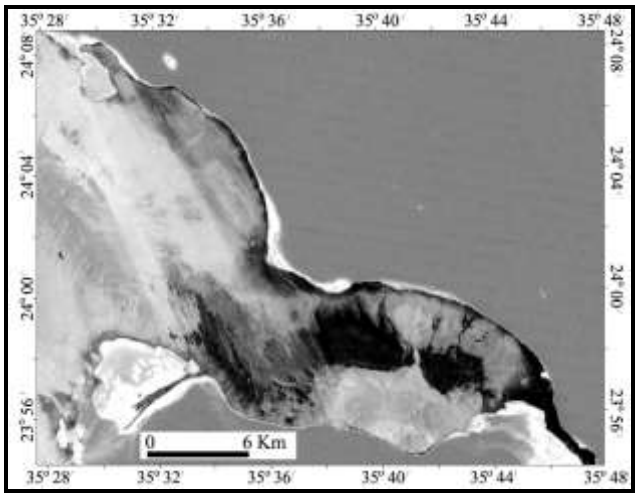

Figure 11. Gray-scale PC3-image shows carbonates with light-gray tone and sulfate-evaporites with dark tone.

The PC2 separates clearly between visible bands (positive eigenvector loadings) and SWIR bands (negative eigenvector loadings). This PC has about 2.8% of the total data variation and shows highest positive loading (0.58) on band2 as well as highest negative loading (-0.54) on band7. It implies that the carbonates and sulfate-evaporites have reflectance features in the visible band2 and absorption features in the infrared band 7. The gray-scale PC2 image (Fig. 10) is obviously able to differentiate between carbonate rocks with dark tone, and sulfate-evaporites with light-gray tone. The PC3 contains about 0.40% of data variance. It has strongly positive loading (0.63) on band7 and negative loading (-0.52) on band5. This PC points to the difference in the spectral behaviour between the carbonates and sulfate-evaporites through the wavelength ranges of bands 5 and 7.

Table 4. Eigenvector loadings and eigenvalues of Crosta PCs.

	PC1	PC2	PC3	PC4
Band 2	0.35	0.58	0.50	0.54
Band 3	0.54	0.49	-0.30	-0.61
Band 5	0.60	-0.37	-0.52	0.49
Band 7	0.47	-0.54	0.63	-0.32
Eigenvalue (Cov.)	7600.70	177.77	29.43	6.21
Information %	96.7	2.8	0.4	0.1

Carbonate rocks have reflectance features in band5 and absorption features in band7, whereas sulfate-evaporites show absorption features in the two bands. Contrasting to PC2 image, the gray-scale PC3 image (Fig. 11) separates between carbonates with light-gray tone, and sulfate-evaporites with dark tone. The PC4 has negative contribution to band3 (-0.61) and positive contribution to band2 (0.54). This PC indicates the spectral behaviour of Fe-bearing minerals that have absorption feature in band1 and reflectance feature in band3. So, such Fe-bearing materials will appear with dark tone on the gray-scale PC4 image.

4.2.3. False Color Composition

Different band ratio combinations are processed in the present study to discriminate between different lithologies of Ras Banas Peninsula. Certain band ratios (e.g. 5/7, 5/1, 5/4 and 3/4) are sensitive to certain chemical and mineralogical compositions of the rocks (e.g. Sultan et al., 1986; Ali-Bik et al., 2012). The processed false colored composite (FCC) band ratios image (5/7:R, 5/1:G, 3/1:B) clearly discriminates the sulfate-evaporites with rose and pinkish image signature (Fig. 12). On the other hand, the carbonate facieses appear with light turquoise color and the metagabbros have dark brown color, whereas the granites show dark green image signature.

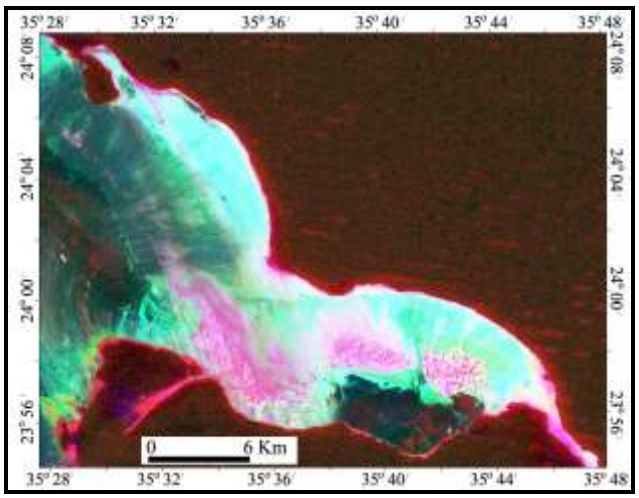

Figure 12. FCC-band ratios image (5/7:R, 5/1:G, 3/1:B) discriminates clearly evaporites with rose and pinkish colors and carbonates with light turquoise color.

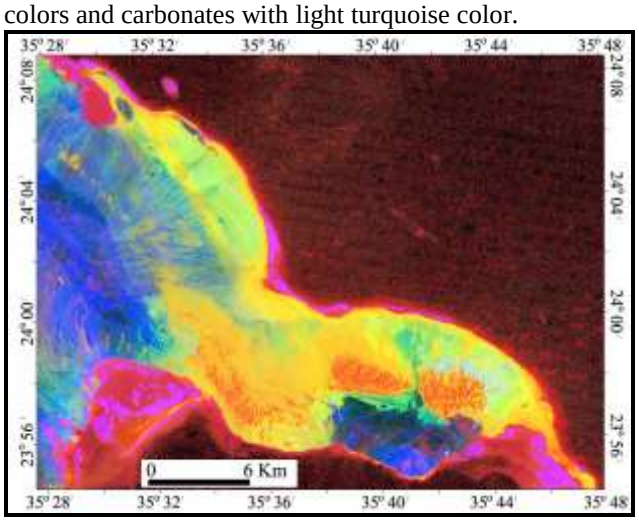

Figure 13. FCC-band ratios image (5/7:R, 5/1:G, 5/4*3/4:B) discriminates clearly evaporites with orange color, dolostone with green color, limestone facies with lemon and light blue colors**.**

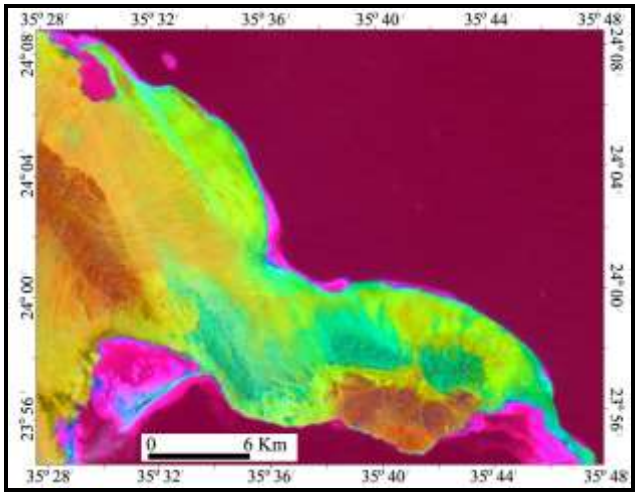

Figure 14. RGB PC-image (PC3, PC1, PC2) discriminates evaporites with turquoise color and carbonates with lemon color, the recent sediments have light-brown colors.

The clastic sediments appear with green and light greenish color. Moreover, the processed FCC band ratios image (5/7:R, 5/1:G, 5/4*3/4:B) is competent to differentiate between all litho-facieses in the study area (Fig. 13). On this image, the evaporites of Abu Dabbab Formation show orange and yellowish red colors. Both the pre-evaporite dolomites of Gebel El Rusas Formation and the post-evaporite dolomites of Um Gheig Formation have greenish image signature, while the limestones of Samh Formation exhibit whitish blue image signature. Limestones of Shagra Formation appear on this FCC image with lemon color, meanwhile silicified limestones of Ras Ranga Formation show dark blue color. The basement complex rocks of Ras Banas Peninsula (Fig 1) include metagabbros and gray granites. Metagabbros appear on this image with purple color, while gray granites have bluish image signature. The clastic sediments of Gebel El Rusas Formation and the recent sediments exhibit light blue and yellowish colors, respectively. Conventionally, because the first three components carry most of the information, the PC1, PC2, and PC3 are displayed as RGB composite for rock-units discrimination. A False color composite image resulted from combination of PC3 in Red channel, PC1 in Green channel and PC2 in Blue channel (Fig. 14). This image differentiates between the rock units covering Ras Banas area.

The sulfate-evaporites appear with turquoise color, while the carbonate rocks have lemon. The basement rocks show brown image signature, meanwhile the recent sediments have light-brown, yellowish and light-turquoise colors.

5. CONCLUSIONS

Tectonically, Ras Banas peninsula is considered as a part of Pre-Miocene continental slope. The Ras Banas sedimentary successions account the sedimentation history from Middle Miocene up to Holocene. In general, the Miocene sediments of the Red Sea coast were deposited mainly in tectonically formed basins; consequently they exhibit frequent unconformities and great facies variations. At Ras Banas Peninsula, there are six unconformity surfaces; the oldest one separates the Precambrian basement rocks from the overlying Middle Miocene sediments. The other unconformity surfaces separate between the different stratigraphic units, supporting cyclic sedimentation in tectonically unstable – at least during lower Middle Miocene- environment.

Based on deformational history that is principally pertaining to the Red Sea rifting event, the sedimentary succession of the study area could be distinguished into two main subdivisions: a) syn-rifting sequences (the lower units of the Middle

Miocene section), and b) post-rifting successions which include the topmost unit of the Middle Miocene section in addition to Upper Miocene, Pliocene, Pleistocene and Holocene sediments.

Based on deformational history that is principally pertaining to the Red Sea rifting event, the sedimentary succession of the study area could be distinguished into two main subdivisions: a) syn-rifting sequences (the lower units of the Middle Miocene section), and b) post-rifting successions which include the topmost unit of the Middle Miocene section in addition to Upper Miocene, Pliocene, Pleistocene and Holocene sediments.

The syn-rifting sequence overlies non-conformably the Precambrian crystalline basement and characterizes by frequent strike-slip and normal steep-dipping to near vertical faults. On the contrary, the post-rifting succession is generally horizontal without any deformational signs, except at the north-western part of the Peninsula, where an anticline is recorded and attributed probably to the plasticity of their underlying evaporites. The syn-rifting, deformed sequences are represented by the mixed siliciclastics/carbonates (Gebel El Rusas Fm) and the evaporites of Abu Dabbab Fm.

The recorded deformational patterns in the Middle Miocene section of Ras Bans area follow – in general - the main ancient faulting trends in the older rocks of the south-eastern part of Egypt. These ancient fractures and shears most probably originated in response to many successive compressive and/or extension forces, since the Precambrian and culminated in the Red Sea rifting.

The mixed siliciclastics/carbonate rock-unit of Gebel El Rusas Fm exhibits variable depositional systems (continental, marine and transitional) and tectonically unstable sub-environments that were greatly impacted by both local tectonic unrest and global sea level-fluctuation. The continental clastic components of this rock-unit imply cycles of sedimentation in different depositional environments. They encompass basal polymictic conglomerates and cycles of fluviatile and intertidal alluvial fan sandstones with intercalation of gypsiferous claystones during prograding muddy shoreline. The basal conglomerates indicate accumulation in high-energy environment. The gravel and other clasts were derived most probably from the nearby crystalline basements, while sandstones seem to be recycled products of pre-existing siliciclastic sources.

The carbonates were deposited in lagoonal depositional system implying calm environment along the shoreline of a siliciclastic continental shelf. The carbonate rocks of Gebel El Rusas Formation are almost totally dolostone with substantial amount of quartz.

The dolostone is most probably evolved at expense of the pre-existing limestone. Dolomitization of the latter could probably be linked with the succeeding evaporites (Abu Dabbab Fm), by the action of the subaerial brine reflux. Geochemically, the samples of Gebel El Rusas Formation (mixed siliciclastics/carbonates) are scattered between the quartz and dolomite reference points, exhibiting heterogeneous composition and supporting the field and microscopic investigations.

The Abu Dabbab evaporites comprise subaerial and subaqueous gypsum and anhydrite deposits, which developed in supratidal sabkha and shoal environments, respectively. Primary gypsum occurs in different forms (tabular and lenticular gypsum) and sizes (selenite and alabaster) implying evolution under varying salinities in environment characterized by microbial bloom. The lenticular-gypsum form is attributed to interaction of biogenic crystallization inhibitors.

The post-rifting successions are started by the Um Gheig Fm, which is composed of almost pure dolostone that implies shallow open marine environment. It is free of quartz in comparison to the syn-rifting siliceous dolostone of Gebel El Rusas Fm. Again, the dolostone was formed by the dolomitization of the pre-existing limestone either by the interaction of meteoric porewaters in a mixing-zone with the marine porewaters (mixing-zone model) or by the involvement of the marine porewaters in response to the sea-level rising.

The Um Gheig Fm is followed upward by Samh Fm (Upper Miocene) which is composed of limestone, stromatolitic limestone and sandy limestone, implying shallow open marine environment. Pliocene sediments are represented by Shagra Formation, which is formed of sandy limestone, coralline and stromatolitic limestones, suggesting foreslope and organic build up environment. The Pleistocene sediments are represented by silicified coral reefs (Ras Ranga Formation), while the Holocene sediments are represented byraised coral reefs, sandy ravels and beach sands. The chemical data as presented is in close agreement with field and microscopic data.

Band rationing technique revealed the impact of diagnostic absorption features of carbonates and evaporites in the infrared ETM bands (band 5, band 7). The band ratio (5/7) is competent to discriminate the carbonate rocks from the evaporites of Ras Banas. The PC2 of Crosta PCA clearly differentiates between the visible and infrared bands. It illustrates the reflectance and absorption features of carbonates

and evaporites through the visible and infrared regions, respectively. Moreover, the PC3 is comparable with the band ratio (5/7), implying the difference in spectral behavior of carbonate rocks and evaporites through the infrared region. The FCC ratio image (5/7:R, 5/1:G, 5/4*3/4:B) is the best ratio combination that can clearly discriminate between all the rock units of Ras Banas area.

ACKNOWLEDGEMENT

The authors are grateful to Prof. Dr. Ovidiu Dragastan for his constructive suggestion and criticism.

REFERENCES

Abdel Gawad, M. 1969. *Geological structures of the Red Sea area inferred from satellite pictures.* In: Degens ET, Ross DA (eds) *Hot brines and recent heavy metal deposits in the Red Sea.* Springer. 25-37.

Abou Elmagd, A. K. & Emam, A. 2012. *Geomorphology and drainage network of Ras Banas Peninsula, Egyptian Red Sea coast: a model of coastal threshold.* Arab J Geosci. DOI 10.1007/s12517-012-0660-0.

Abrams, M.J. & Hook, S.J. 1995. *Simulated ASTER data for geologic studies.* IEEE Trans. Geoscience and Remote Sensing, 33, 692–699.

Akkad, S.E & Dardir, A. 1966. *Geology of the Red Sea Coast between Ras Shagra and Mersa Alam with short notes on exploratory work at Gebel El-Rusas lead-zinc deposits.* Geol. Surv. Egypt, Paper 35, 67 pp.

Al Rawashdeh, S., Saleh, B. & Hamzah, M. 2006. *The use of remote sensing technology in geological investigation and mineral detection in El Azraq-Jordan.* Cybergeo: European Journal of Geography 358. http://www.cybergeo.eu/index 2856.html.

Ali-Bik, M.W, Metwally, I.M., Kamel, M.G. & Wali, A.M.A. 2011. *Gypsum and dolomite biomineralization in endoevaporitic microbial niche, EMISAL, Egypt.* Environ Earth Sci. 62, 151-159.

Ali-Bik, M.W., Taman, Z., El Kalioubi, B. & Abdel Wahab, W. 2012. *Serpentinite-hosted talc-magnesite deposits of Wadi Barramiya area, Eastern Desert, Egypt: Characteristics, petrogenesis and evolution.* J. Afr. Earth Sci. 64, 77-89.

Beadnell, H.J.L. 1924. *Report on the geology of the Red Sea Coast between Quseir and Wadi Ranga.* Petrol. Res. Bull. 13, Cairo. 37pp.

Boggs, S.Jr. 2001. *Principles of Sedimentology and Stratigraphy.* 3rd edition, Prentice Hall, 726 pp.

Chavez, P.S. 1989. *Extracting spectral contrast in Landsat Thematic Mapper image data using selective principal component analysis.* Photogrammetric Engineering and Remote Sensing 3, 339-348.

Cody, A.M. & Cody, R.D. 1989. *Evidence for micro-biological induction of [101] Montmartre twinning of gypsum (Ca SO_4. $2H_2O$).* J. Crystal Growth. 98, 721-730.

Crosta, A.P. & Moore, J.Mc.M. 1989. *Enhancement of Landsat Thematic Mapper imagery for residual soil mapping in SW Minas Gerais State Brazil: a prospecting case history in greenstone belt terrain. Proceeding of the 9th Thematic Conf. Remote Sensing for Exploration Geology, Calgary (Ann Arbor, MI:* Environmental Research Institute of Michigan), pp. 1173-1187.

Crowley, J.K. 1986. *Visible and near-infrared spectra of carbonate rocks: Reflectance variations related to petrographic texture and impurities:* J. Geophys. Res., 91, 5001-5012.

Felesteen, A.W., Khedr, E.S. & Ali, K.A. 1994. *The Neogene- Quaternary sequence of Ras Banas Peninsula: (1) Stratigraphical studies.* Egypt. J. Geol., 38, 267-287.

Gad, S. & Kusky, T.M. 2007. *ASTER spectral ratioing for lithological mapping in the Arabian-Nubian Shield, the Neoproterozoic Wadi Kid area, Sinai, Egypt.* Gondwana Research 11, 326–335.

Gaffey, S.J. 1985. *Reflectance spectroscopy in the visible and near infrared (0.35-2.55 microns): Applications in carbonate petrology.* Geology, 13, 270-273.

Gaffey, S.J. 1986. *Spectral reflectance of carbonate minerals in the visible and near-infrared (0.35-2.55 microns): Calcite, aragonite, and dolomite.* Am. Mineral., 71, 151-162.

Gaffey, S.J. 1987. *Spectral reflectance of carbonate minerals in the visible and near-infrared (0.35-2.55 microns): Anhydrous carbonate minerals*. J. Geophys. Res, 92, 1429-1440.

Girdler, R.W. 1969. *The Red Sea-a geophysical background*. In: Degens ET, Ross DA (eds) *Hot brines and recent heavy metal deposits in the Red Sea.* Sringer, pp. 38–58.

Gupta, R.P. 2003. *Remote Sensing Geology.* Springer, Heidelberg, 655 pp.

Haq, B.U., Hardenbol, J. & Vail, P.R. 1987. Chronology of fluctuating sea levels since the Triassic. Science, 235, 1156-1167.

Howari, F. 2002. *Spectroscopy of evaporites, Periodico di Mineralogia,* An International Journal of Mineralogy, Crystallography and Geochemistry, 71, 191–200.

Huang, C.K. & Kerr, P.F. 1960. *Infrared study of the carbonate minerals.* Am. Mineral., 45, 311-324.

Hunt, G.R. 1982. *Spectroscopic Properties of Rocks and Minerals.* In: Carmichael RS (ed) *Handbook of Physical Properties of Rock.* CRC Press, Boca Raton, Vol. I, pp. 295-385.

Hunt, G.R. & Salisbury, J.W. 1970. *Visible and near infrared spectra of minerals and rocks. I. Silicate minerals.* Modern Geology, 1, 283-300.

Hunt, G.R. & Salisbury, J.W. 1971. *Visible and near infrared spectra of minerals and rocks: II. Carbonates.* Modern Geology, 2, 23-30.

Inzana, J., Kusky, T.M., Higgs, G. & Tucker, R. 2003. *Supervised classifications of Landsat TM band ratio images and Landsat TM band ratio image with radar for geological interpretations of central*

Madagascar. J. Afr. Earth Sciences 37, 59–72.

Jensen, J.R. 1986. *Introductory digital image processing: A remote sensing perspective.* Prentice-Hall, Englewood Cliffs, New Jersey, 379 pp.

Khedr, E.S. 1984. *Sedimentological evolution of the Red Sea continental margin of Egypt and its relationship to sea level changes.* J. Sed. Geology, 39, 71-86.

Kusky, T.M. & Ramadan, T.M. 2002. *Structural controls on Neoproterozoic mineralization in the South Eastern Desert, Egypt: an integrated field, Landsat TM and SIR-C/X SAR approach.* J. Afr. Earth Sci., 35, 107-121.

Loughlin, W.P. 1990. *Geological Exploration in the Western United States by Use of Airborne Scanner Imagery. IMN Conf. "Remote Sensing* – An Operational Technology for Mining and Petroleum", London, Oct. 29-31, 1990, pp. 223-241.

Loughlin W.P. 1991. *Principal components analysis for alteration mapping.* Photogrammetric Engineering and Remote Sensing, 57, 1163–1169.

Madani, A. & Emam, A. 2011. *SWIR ASTER band ratios for lithological mapping and mineral exploration: a case study from El Hudi area, southeastern desert, Egypt.* Arab J Geosci, 4, 45-52.

Mahran, T.M. 2000. *Cyclicity and sequence stratigraphy of syn-rift Late Neogene mixed carbonate-siliciclastics of the area between Wadi Zug El Bohar and Wadi Dabr, Red Sea, Egypt.* Egypt. J. Geol., 44(2), 237-275.

Meshref, W.M. 1990. *Tectonic framework. In: Said R (ed) The Geology of Egypt*. A. A. Balkema, Rotterdam, Brookfield, pp. 113-155.

Philobbos, E.R., El-Haddad, A.A. & Mahran, T.M. 1988. *Comparison between Miocene and Pliocene facies distribution related to syn-rift tectonics along the Egyptian Red Sea Coastal Area*. Egyptian general Petroleum Co., 9th Petroleum Exploration Seminar, Cairo, Printed (1990), V.1, p. 246-254.

Ranjbar, H., Honarmand, M. & Moezifar, Z. 2004. *Application of the Crosta technique for porphyry copper alteration mapping, using ETM+ data in the southern part of the Iranian volcanic sedimentary belt.* J. Asian Earth Sci. 24, 237–243.

Roser, B.P. & Korsch, R.J. 1988. *Provenance signatures of sandstones-mudstone suites determinated using discriminant function analysis of major-element data*. Chem. Geol., 67, 119-139.

Sabins, F.F. 1997. *Remote Sensing - Principles and Interpretation,* 3rd ed., W.H. Freeman, New York, 494 pp.

Said, R. 1962. *The geology of Egypt.* Elsevier, 377 pp.

Said, R. 1990. *Quaternary*. In: Said R (ed) *The Geology of Egypt*. A. A. Blakema, Rotterdam, Brookfield, pp. 487-507.

Samuel, M.D. & Cherif, O.H. 1978. *An approach to the study of paleoclimatic and tectonic control of sedimentation of some Neogene rocks along the Red Sea coast, Egypt*. Bull. Nat. Res. Council, Cairo 3, 209-215.

Samuel, M.D. & Saleeb-Roufaiel, G.S. 1977. *Lithostratigraphy and petrographic analysis of the Neogene sediments at Abu Ghusun, Um Mahara Area, Red Sea Coast, Egypt.* Beitr. Zur Lithologie, Freiburg Forsch. 323(c). 45-56.

Sanz-Montero, M.E., Rodrigues-Aranda, J.P. & Calvo, J.P. 2005. *Biomineralization in relation with endoevaporitic microbial communities. Miocene Lake deposits of Madrid Basin, Central Spain.* Geophys. Res Abstract. 7, 06837. SRef-ID: 1607-7962/gra/EGU05-A-06837. European Geosciences Union.

Schandelmeier, H., Klitzsch, E., Hendriks, F. & Wycisk, P. 1987. *Structural development of North-East Africa since Precambrian Times*. In: Klitzsch E, Schrank (eds) *Results of the Special Research Project Arid Areas Period 1984 - 1987.* Berliner Geowiss. Abh., 75, 5-24.

Singh, A. & Harrison, A. 1985. *Standardized principal components*. Int. J. Remote Sens. 6, 883–896.

Sultan, M., Arvidson, R.E. & Sturchio, N.C. 1986. *Mapping of serpentinites in the Eastern Desert of Egypt using Landsat thematic mapper data.* Geology, 14, 995–999.

Van der Meer, F. 1994. *Sequential indicator conditional simulation and indicator kriging applied to discrimination of dolomitization in GER 63-channel imaging spectrometer data.* Nonrenewable Resources, 3, 146–164.

Van der Meer, F. 1995. *Spectral reflectance of carbonate mineral mixtures and bidirectional reflectance theory: Quantitative analysis techniques for application in remote sensing.* Remote Sensing Review, 13, 67–94.

Wilson, J.L. 1975. *Carbonate facies in geological history.* Springer-Verlag, Berlin, Heidelberg, New York, 471 pp.

Wimmenauer, W. 1984. *The pre Variscan crystalline basement of the Black Forest. In German.* Fortschritte Mineralogie Beiheft, 62, 69-86.

Wintsch, R.P. & Kvale, C.M. 1994. *Differential mobility of elements in burial diagenesis of siliciclastic rocks.* J. Sed. Res., A64, 349-361.

Received at: 20. 02. 2013
Revised at: 31. 05. 2013
Accepted for publication at: 07. 06. 2013
Published online at: 13. 06. 2013